Cell Insight 3 (2024) 100170

Contents lists available at ScienceDirect

Cell Insight

journal homepage: www.journals.elsevier.com/cell-insight

Research Article

LUC7L3 is a downstream factor of SRSF1 and prevents genomic instability

Xiaqing Zhang [a,b], Jing Guo [a,b], Xin Shi [a,b], Xin Zhou [a,b], Qiang Chen [a,b,c,d,e,*]

[a] Department of Gastrointestinal Surgery, Medical Research Institute, Zhongnan Hospital of Wuhan University, Wuhan University, Wuhan, 430071, China
[b] Frontier Science Center for Immunology and Metabolism, Medical Research Institute, Wuhan University, Wuhan, 430071, China
[c] Clinical Medical Research Center of Peritoneal Cancer of Wuhan, Wuhan, 430071, China
[d] Hubei Key Laboratory of Tumor Biological Behaviors, Zhongnan Hospital of Wuhan University, Wuhan, 430071, China
[e] Hubei Province Cancer Clinical Study Center, Zhongnan Hospital of Wuhan University, Wuhan, 430071, China

HIGHLIGHTS

- LUC7L3 depletion impairs cell proliferation compared to other Luc7p paralogs, leading to cell apoptosis and senescence.
- LUC7L3 depletion leads to the accumulation of R-loops, which are RNA-DNA hybrids that can cause DNA replication stress and genome instability.
- LUC7L3 depletion causes abnormalities in spindle assembly, resulting in the formation of multinuclear cells.
- SRSF1 positively regulates LUC7L3 protein translation.

GRAPHICAL ABSTRACT

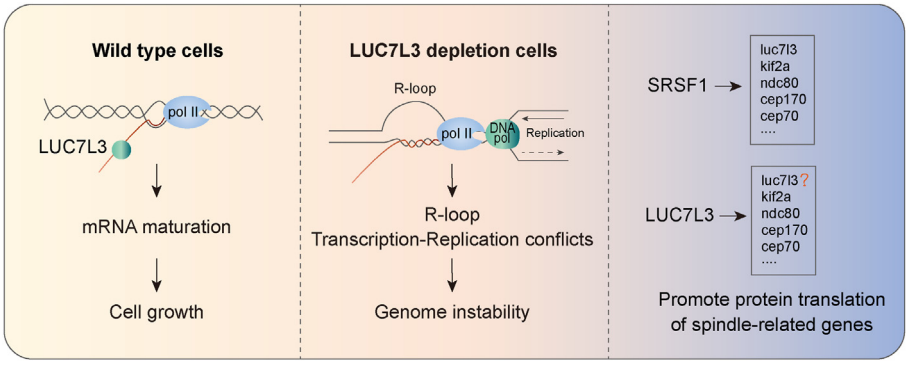

ARTICLE INFO

Keywords:
LUC7L3
SRSF1
R-loop
Genome stability

ABSTRACT

The RNA-binding protein LUC7L3 is the human homolog of yeast U1 small nuclear RNA (snRNA)-related splicing factor Luc7p. While the primary function of LUC7L3 as an RNA-binding protein is believed to be involved in RNA metabolism, particularly in the splicing process, its exact role and other functions are still not fully understood. In this study, we aimed to elucidate the role of LUC7L3 and its impact on cell proliferation. Our study revealed that LUC7L3 depletion impairs cell proliferation compared to the other Luc7p paralogs, resulting in cell apoptosis and senescence. We explored the underlying mechanisms and found that LUC7L3 depletion leads to R-loop accumulation, DNA replication stress, and genome instability. Furthermore, we discovered that LUC7L3 depletion caused abnormalities in spindle assembly, leading to the formation of multinuclear cells. This was attributed to the dysregulation of protein translation of spindle-associated proteins. Additionally, we investigated the interplay between LUC7L3 and SRSF1 and identified SRSF1 as an upper stream regulator of LUC7L3, promoting the translation of LUC7L3 protein. These findings highlight the importance of LUC7L3 in maintaining genome stability and its relationship with SRSF1 in this regulatory pathway.

* Corresponding author. Department of Gastrointestinal Surgery, Medical Research Institute, Zhongnan Hospital of Wuhan University, Wuhan University, Wuhan, 430071, China.
E-mail address: Chenq124@whu.edu.cn (Q. Chen).

https://doi.org/10.1016/j.cellin.2024.100170
Received 29 January 2024; Received in revised form 14 March 2024; Accepted 19 March 2024
Available online 23 March 2024

1. Introduction

Vertebrates possess three yeast Luc7p paralogs, namely LUC7L, LUC7L2, and LUC7L3. These proteins comprise the N-terminal alpha-helix domain, ZnF domains, and C-terminal arginine-serine-rich (RS) domains (Daniels et al., 2021; Howell et al., 2007). Yeast Luc7p plays a crucial role in pre-mRNA splicing, and perturbations in its N-terminal structural domain or mutations/deletions of ZnF1 can result in impaired splicing events *in vivo*. Additionally, mutation of ZnF2 can lead to a lethal phenotype (Agarwal et al., 2016). Recently, Daniels et al. have extensively investigated the functions of LUC7L, LUC7L2, and LUC7L3 in relation to their associated proteins, RNA crosslinking site profiles, and roles in RNA splicing (Daniels et al., 2021). Their findings indicate that LUC7L2 and LUC7L3 exhibit distinct characteristics compared to LUC7L. For instance, while LUC7L predominantly associates with hnRNP proteins, both LUC7L2 and LUC7L3 bind with SR proteins. Additionally, whereas LUC7L primarily crosslinks with intronic sequences, both LUC7L2 and LUC7L3 are predominantly bound to exonic sequences. Notably, LUC7L2 can repress OXPHOS and promote glycolysis by regulating specific gene alternative splicing (Jourdain et al., 2021). Furthermore, LUC7L2 can directly bind to intron 3 of MITA/STING precursor mRNA and regulate innate antiviral response (Li et al., 2021). However, the role of LUC7L3 remains elusive. The LUC7L3 gene was initially identified as a novel RS nuclear protein in cisplatin-resistant cell lines (Nishii et al., 2000). *In vitro* studies have shown that LUC7L3 is phosphorylated by mSRPK1, mSRPK2 and Clk1, and Clk1 phosphorylation of SR proteins alters splicing (Prasad et al., 1999). RBM25 binds to the exonic shear enhancer CGGGCA, potentially stabilizing precursor mRNA-U1 snRNP through interaction with LUC7L3, and activating shearing at the 5′ shear site of pro-apoptotic factor Bcl-Xs (Zhou et al., 2008). Both RBM25 and LUC7L3 may regulate alternative splicing of Na + channel transcript which could be associated with heart failure (Gao et al., 2011, 2013). Herein, this study reveals that depletion of LUC7L3 leads to significant growth defects, unlike individual depletions of either LUC7L or LUC7L2. We further demonstrate that LUC7L3 prevents R-loop accumulation and promotes spindle assembly thereby contributing to maintaining genomic stability.

R-loops are unique structures formed by the invasion of RNA into double-stranded DNA, resulting in the formation of a triple-stranded nucleic acid structure (Roberts et al., 1992; Thomas et al., 1976) While R-loops have beneficial effects in certain physiological contexts, their abnormal accumulation can lead to DNA damage and genomic instability. This occurs through the inhibition of replication fork progression and the promotion of double-strand breaks (Gan et al., 2011; Niehrs et al., 2020). Unscheduled R-loop formation is associated with increased DNA breaks, transcription-replication collisions, mutagenesis, and chromosomal rearrangements, resulting in genome instability (Aguilera et al., 2012; Hamperl et al., 2014, 2017). Several proteins, including topoisomerases (Tuduri et al., 2010; Yang et al., 2014), splicing factors (Li et al., 2005) and chromatin regulators (Bayona-Feliu et al., 2021), act to prevent R-loop formation during transcription. Splicing factors, such as SRSF1 and SRSF2, which contain RS domains, play a crucial role in this process. SRSF1 is particularly important for maintaining genomic stability by preventing the formation of RNA-DNA hybrid R-loop structures (Li et al., 2005). Mutations in high-risk alleles of the splicing factors SRSF2 and U2AF1 have been found to increase R-loop levels, replication stress, and activate the ATR-CHK1 signal pathway (Chen et al., 2018). In addition to splicing factors, other proteins such as RNase H (Wahba et al., 2011), DNA: RNA helicase enzymes like DDX18 (Lin et al., 2022), DDX5 (Yu et al., 2020), DHX9 (Chakraborty et al., 2018), and RNA binding and processing proteins (Bhatia et al., 2014) have been identified as regulator of R-loop accumulation. These proteins play a crucial role in maintaining R-loop homeostasis and preserving genome stability *in vivo*.

Here, we uncovered that depletion of LUC7L3 resulted in the accumulation of R-loops and DNA replication stress, leading to genomic instability characterized by chromosome breaks and micronuclei formation. Apart from its role in RNA splicing, LUC7L3 also plays a role in the regulation of protein translation, facilitating spindle assembly during mitosis. Furthermore, the efficiency of LUC7L3 protein translation was found to be influenced by SRSF1, a protein involved in RNA processing. SRSF1 positively regulated LUC7L3 protein levels, suggesting that LUC7L3 may be a downstream factor of SRSF1.

2. Results

2.1. LUC7L3 depletion impairs cell proliferation

The function of the mammalian LUC7-like family of proteins on cell survival remains elusive. To investigate the functional role of LUC7-like protein on cell survival, we depleted LUC7L, LUC7L2, and LUC7L3 using short hairpin RNAs (shRNA) (Supplemental Fig. 1A). Depletion of LUC7L3 significantly decreased cell proliferation in A549 and HeLa cells, whereas depletion of LUC7L and LUC7L2 had no such effect (Fig. 1A). Moreover, this decrease in cell proliferation was accompanied by an increase in apoptotic cell death (Fig. 1B, Supplemental Fig. 1C) and cellular senescence (Fig. 1C, Supplemental Fig. 1D). These findings were further supported by colony formation assays (Supplemental Fig. 1B), suggesting that LUC7L3 exhibits distinct functions related to cell survival compared to LUC7L and LUC7L2. Considering the collaborative role of LUC7L3 and RBM25 in mRNA alternative splicing (Le Sénéchal et al., 2023; Zhou et al., 2008), we explored whether knockdown of RBM25 would elicit similar effects as observed upon depletion of LUC7L3. Interestingly, depletion of RBM25 did not significantly affect cell proliferation (Fig. 1A), indicating that LUC7L3 may have unknown functions associated with its role in promoting cell survival.

LUC7L3 depletion resulted in robust DNA damage in HeLa cells, as evidenced by the increased phosphorylation of histone variant H2AX (γH2AX) (Khanna et al., 2001; Mah et al., 2010; Redon et al., 1999; Rogakou et al., 1998) and KAP1 (p-KAP1), which are established biomarkers for DNA damage (Fig. 1D) (White et al., 2006; Ziv et al., 2006). In contrast, depletion of LUC7L, LUC7L2 or RBM25 did not induce DNA damage. Immunofluorescence staining (IF) revealed a significant increase in γH2AX foci upon LUC7L3 depletion in both HeLa and A549 cells (Fig. 1E). Moreover, we observed that chromosomal instability markers, such as micronuclei and nucleoplasmic bridges, were elevated in LUC7L3-depleted A549 cells (Fig. 1F and G). Collectively, these results indicated that LUC7L3 depletion led to DNA damage and genomic instability, which may contribute to impaired cell proliferation. Intriguingly, we also discovered that LUC7L3 depletion induced the accumulation of multinuclear cells, which may also contribute to the decreased cell proliferation following its loss (Fig. 1H).

2.2. LUC7L3 prevents R-loop-induced accumulation of DNA damage

As splicing factors act to prevent R-loop formation during RNA transcription, and unscheduled R-loops lead to DNA damage and genomic instability after splicing factor depletion (Goulielmaki et al., 2021; Jimenez et al., 2019; Jin et al., 2023; Li et al., 2005), we speculated that LUC7L3 depletion may lead to aberrant R-loop formation. To investigate whether LUC7L3 depletion leads to aberrant R-loop formation, we monitored R-loops using the S9.6 antibody, which specifically detects DNA-RNA hybrids (Boguslawski et al., 1986; Bou-Nader et al., 2022). SRSF1-depleted cells served as the positive control for the enrichment of R-loop (Li et al., 2005, 2007). We observed a significant enrichment of the S9.6 signal in LUC7L3-depleted A549 cells, similar to what was observed in SRSF1-depleted cells (Fig. 2A). In contrast, depletion of LUC7L2 did not result in the enrichment of the S9.6 signal (Supplemental Fig. 2A). Moreover, we observed the accumulation of R-loops in different cell lines, including HeLa, U2OS, and non-transformed hTERT RPE-1 cells, upon LUC7L3 depletion (Fig. 2B, Supplemental Figs. 2B and C). Treatment with DRB, which inhibits gene transcription (Chodosh et al., 1989; Yankulov et al., 1995), diminished

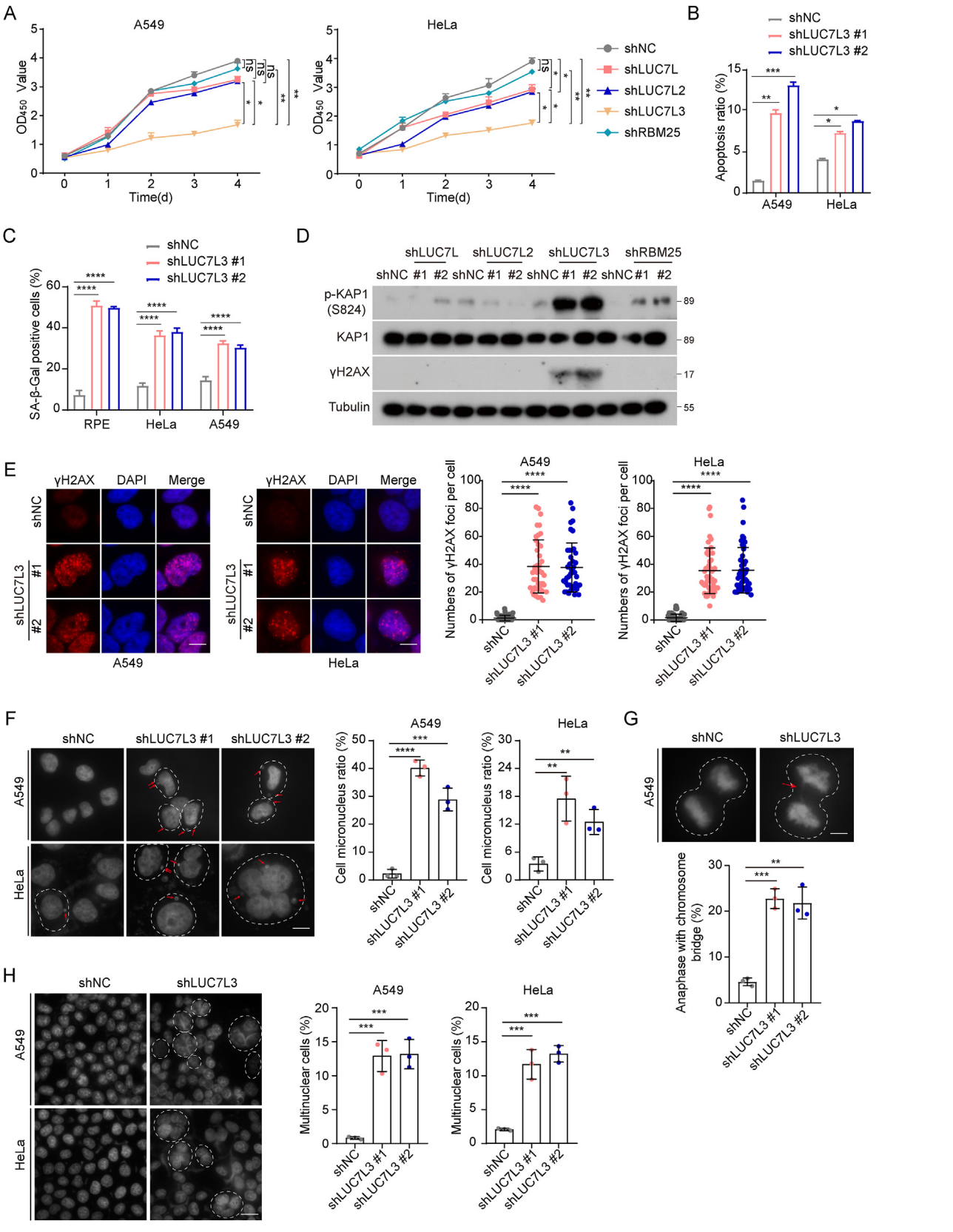

(caption on next page)

Fig. 1. Impact of LUC7L3 depletion on cell proliferation

A. Knockdown of LUC7L, LUC7L2, LUC7L3, and RBM25 proteins in A549 and HeLa cell lines. Cell viability was assessed using the CCK-8 assay.

B. Flow cytometry analysis of apoptosis in LUC7L3-interfered A549 and HeLa cells.

C. Detection of senescence-associated β-galactosidase (SA-β-Gal)-positive cells in LUC7L3-interfered RPE, A549, and HeLa cells using a cellular senescence kit.

D. Western blot analysis of γH2AX, KAP1, and p-KAP1 (S824) protein levels in A549 cells following knockdown of LUC7-like proteins LUC7L, LUC7L2, LUC7L3, and RBM25.

E. Immunofluorescence analysis of γH2AX nuclear foci in LUC7L3-knockdown A549 and HeLa cells. Red fluorescence indicates γH2AX, and blue indicates the nucleus with DAPI staining. The number of γH2AX foci per cell was analyzed using Image J software and statistical analysis was performed using GraphPad Prism 8.0.1 software. $n > 70$.

F. Immunostaining of intracellular micronuclei using DAPI in LUC7L3-depleted A549 and HeLa cells. Red arrow: micronuclei. Statistical analysis of the number of micronuclei cells was shown. $n > 100$.

G. Anaphase cells of LUC7L3 deleted A549 cells were immunostained with DAPI. Statistical analysis of the number of nucleoplasmic bridge cells was shown. Red arrow: chromosome bridge. $n > 100$.

H. Immunostaining of multinuclear cells with DAPI in LUC7L3-depleted cells. Dashed red circle: multinuclear cells. Statistical analysis of the number of multinucleated cells was shown. $n > 100$. *$p < 0.05$, **$p < 0.01$, ***$p < 0.001$, ****$p < 0.0001$, indicating statistical significance and ns indicates non-significance. Scale bar: 10 μm. Dash lines outlined cells with micronucleus or multinuclear cells.

the enrichment of the S9.6 signal after LUC7L3 depletion (Fig. 2C and E). Additionally, overexpressing GFP-RNase H1, which specifically degrades DNA-RNA hybrids (Cerritelli et al., 2009, 2022; Stein et al., 1969), abolished the accumulation of the S9.6 signal induced by LUC7L3 depletion (Fig. 2D and E). These findings collectively indicate that LUC7L3 depletion induces the accumulation of R-loops.

As R-loop accumulation will disrupt the DNA replication process through gene transcription and DNA replication head-on collision (Hamperl et al., 2017; Yang et al., 2022), we investigated whether LUC7L3 depletion affects DNA replication speed using a DNA fiber assay (Halliwell et al., 2020; Michalet et al., 1997; Técher et al., 2013). Interestingly, knockdown of LUC7L3 resulted in a significant reduction in DNA replication speed, which could be rescued by overexpressing GFP-RNase H1 (Fig. 3A). Previous studies indicated that the disruption of the DNA replication process by R-loop will activate the ATR-CHK1 pathway (Hodroj et al., 2017; Matos et al., 2020; Prendergast et al., 2020). Next, we examined CHK1 S345 phosphorylation, a marker of DNA replication stress, and found that it was increased after LUC7L3 depletion (Fig. 3B). Importantly, the increase in CHK1 S345 phosphorylation was observed in LUC7L3-depleted cells but not RBM25-depleted cells (Fig. 3C). Notably, overexpression of GFP-RNase H1 prevented CHK1 phosphorylation induced by LUC7L3 depletion (Fig. 3D). These results indicate that LUC7L3 depletion-induced R-loop accumulation leads to DNA replication stress.

Furthermore, overexpressing GFP-RNase H1 reduced γH2AX signals, a marker of DNA damage, in LUC7L3-depleted HeLa and A549 cells (Supplemental Figs. 3A and B). Given that increased DNA replication stress induces chromosome breaks in mitotic cells (Chakraborty et al., 2020; Minocherhomji et al., 2015), we examined the impact of LUC7L3 deficiency on chromosome stability. Consistent with the functional results in Fig. 3A, LUC7L3 depletion resulted in a substantial increase in chromosome breaks, which could be rescued by overexpressing GFP-RNase H1 (Fig. 3E). Thus, we concluded that LUC7L3 depletion-induced R-loop accumulation disrupted the DNA replication process, which caused DNA damage and genome instability.

2.3. *LUC7L3 depletion induces defects in spindle assembly during mitosis*

As shown in Fig. 1H, LUC7L3 depletion also resulted in the formation of aberrant multinuclear cells (Fig. 1H), which could not be rescued by overexpression of GFP-RNase H1 (Fig. 4A). This suggested that LUC7L3 depletion-induced multinuclear cell formation was not solely due to R-loop accumulation. Since LUC7L3 interacts with SRSF1 (Umehara et al., 2003) and SRSF1 depletion could induce multipolar spindle formation, we speculated that LUC7L3 depletion may affect spindle assembly and consequently lead to multinuclear cell formation. To test this hypothesis, we performed an IF assay with mitotic cells to visualize spindle assembly. Control cells exhibited two spindle poles, as indicated by the localization of pericentrin, a protein that accumulates at the spindle pole in mitotic cells (Fig. 4B). In contrast, LUC7L3 depletion dramatically increased the formation of multipolar spindles, characterized by the presence of multiple pericentrin dots (Fig. 4B and C). This effect was rescued by the ectopic expression of LUC7L3 (Fig. 4C), suggesting a role for LUC7L3 in modulating spindle assembly during mitosis. Importantly, the depletion of LUC7L2 did not induce multipolar spindle formation, suggesting that this effect is specific to LUC7L3 (Supplemental Fig. 4A).

Considering that SRSF1 is known to regulate spindle assembly by promoting the translation efficiency of spindle-associated proteins (Maslon et al., 2014), we investigated whether LUC7L3 regulated spindle assembly through the same mechanism. We found that LUC7L3 depletion decreased the protein level of CEP70, CEP170, and KIF2A, which are spindle-associated proteins. This effect was particularly pronounced in nocodazole-treated synchronized mitotic cells (Fig. 4D). IF experiment also showed that LUC7L3 depletion decreased the intensity of CEP170 on centrosomes in interphase cells and spindle poles in mitotic cells (Fig. 4E). To determine whether LUC7L3 depletion induced a decrease of spindle-associated proteins, we performed polysome profiling assay by separating ribosomes using sucrose gradient centrifugation. We measured the ratio of indicated mRNA in polysome fractions and sub-polysome fractions, which reflects the protein translation efficiency of these spindle-associated proteins (Supplemental Fig. 4B) (Maslon et al., 2014). We found that the translation efficiency of CEP70, CEP170, and KIF2A was significantly impaired following LUC7L3 knockdown (Fig. 4F). Conversely, the ectopic expression of SFB-LUC7L3 increased the protein level and translation of these spindle-associated proteins (Fig. 4F and G), indicating that LUC7L3 could promote the translation of CEP70, CEP170, and KIF2A. Thus, these results suggest that LUC7L3 regulates the translation of spindle-associated proteins, similar to the role of SRSF1.

2.4. *SRSF1 depletion causes a decrease in the LUC7L3 protein level*

Surprisingly, we observed a significant decrease in LUC7L3 protein level after SRSF1 depletion in various cell lines (Fig. 5A). In contrast, the LUC7L2 protein level remained unchanged after SRSF1 depletion (Supplemental Fig. 5A). However, the mRNA level of LUC7L3 was not affected by SRSF1 depletion (Fig. 5B), indicating that SRSF1 depletion may not affect the transcription of LUC7L3. Additionally, LUC7L3 depletion did not have an impact on the SRSF1 protein level (Fig. 5C).

To investigate the mechanism behind the SRSF1 depletion-induced decrease in LUC7L3 protein levels, we examined the involvement of proteasome and lysosome-mediated protein degradation. However, treatment with the proteasome inhibitor MG132 or the lysosome inhibitor CQ did not rescue the decrease in LUC7L3 protein levels caused by SRSF1 depletion (Fig. 5D). This suggests that SRSF1 depletion does not affect the stability of the LUC7L3 protein. Since SRSF1 is known to regulate protein translation (Maslon et al., 2014), we next examined the effect of SRSF1 depletion on the translation efficiency of LUC7L3. By

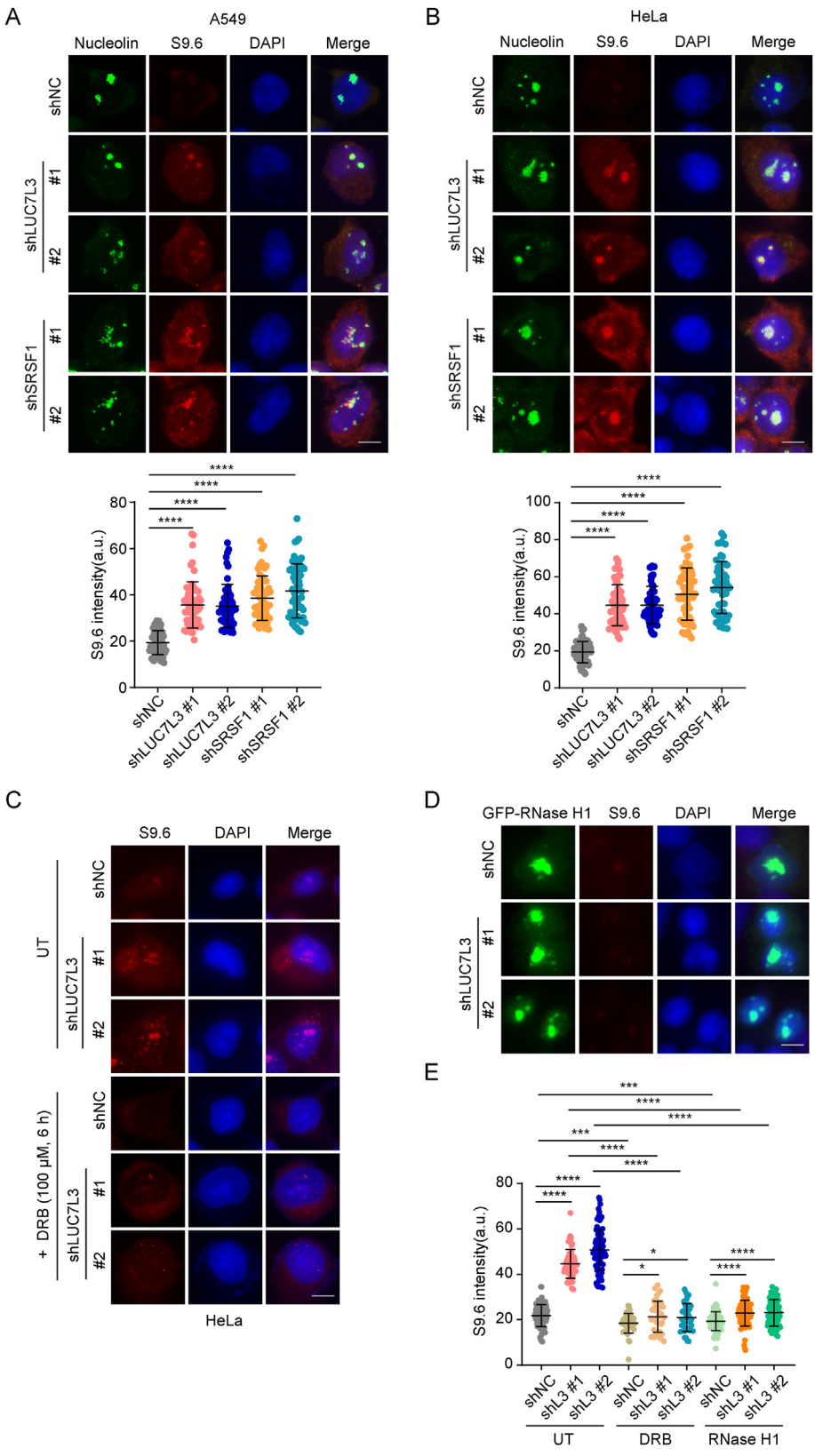

Fig. 2. Accumulation of R-loops following LUC7L3 depletion

A. Immunofluorescence analysis of R-loops in LUC7L3-knockdown A549 cells. SRSF1 depletion cells were used as a positive control. The R-loop was immunostained with S9.6 antibody (Red). The nucleolus was labeled with nucleolin (Green). The nucleus stained with DAPI. The fluorescence intensity of the R-loop was analyzed using Image J software, and statistical analysis was shown. $n > 100$. a. u. means arbitrary units.

B. Immunofluorescence analysis of R-loops in LUC7L3-knockdown HeLa cells as in A.

C. Immunofluorescence analysis of cellular R-loops following treatment with the transcriptional repressor DRB in HeLa cells.

D. Immunofluorescence analysis of intracellular R-loops following overexpression of GFP-RNase H1 in HeLa cells.

E. Statistical analysis of R-loop fluorescence intensity following indicated treatment was shown. $n > 100$. a. u. means arbitrary units. $^{*}p < 0.05$, $^{**}p < 0.01$, $^{***}p < 0.001$, $^{****}p < 0.0001$, indicating statistical significance and ns indicates non-significance. Scale bar: 10 μm.

separating ribosomes using sucrose gradient centrifugation, we measured the ratio of LUC7L3 mRNA in polysome fractions and sub-polysome fractions, which reflects the protein translation efficiency of LUC7L3 (Maslon et al., 2014). As expected, knockdown of SRSF1 resulted in a significant decrease in LUC7L3 protein translation efficiency, while the translation efficiency of LUC7L2 protein remained unaffected (Fig. 5E). Furthermore, overexpression of SRSF1 increased the translation efficiency of LUC7L3 protein (Fig. 5F), leading to an increase in LUC7L3

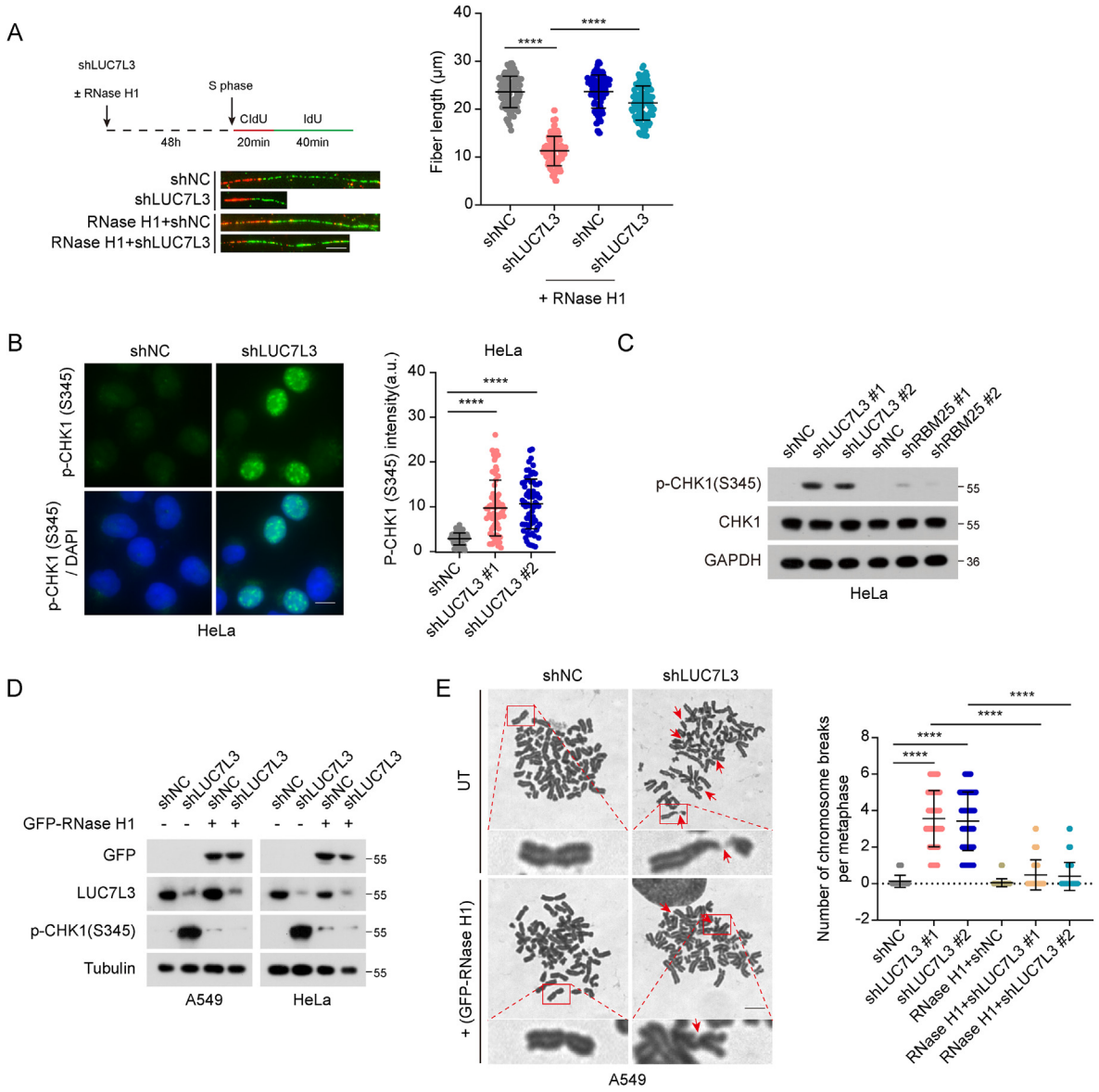

Fig. 3. DNA replication stress and genome instability following LUC7L3 depletion

A. DNA replication speed was analyzed through DNA fiber assay in LUC7L3-depleted A549 cells following indicated treatment. ImageJ software was used for analysis of DNA replication fork length, and statistical analysis was shown. n > 100.

B. Immunofluorescence analysis of p-CHK1(S345) phosphorylation levels in LUC7L3-knockdown HeLa cells. Green fluorescence indicated p-CHK1(S345), and blue represented the nucleus stained with DAPI. Intranuclear fluorescence signals of p-CHK1(S345) were analyzed using ImageJ, and statistical analysis was shown. $n > 70$. a. u. means arbitrary units.

C. Western blot analysis of p-CHK1(S345) and CHK1 protein phosphorylation levels in LUC7L3-and RBM25-depleted HeLa cells.

D. Western blot analysis of p-CHK1(S345) phosphorylation levels in LUC7L3-depleted and GFP-RNase H1-overexpressing A549 and HeLa cells.

E. Chromosome spreading assay to assess the effect of LUC7L3 depletion on chromosomes in A549 cells. $n > 40$. $^{*}p < 0.05$, $^{**}p < 0.01$, $^{***}p < 0.001$, $^{****}p < 0.0001$, indicating statistical significance and ns indicates non-significance. Scale bar: 10 μm.

protein levels (Fig. 5G). Consistent with these findings, IF staining showed an increase in LUC7L3 protein levels in cells overexpressing SRSF1 (Fig. 5H), further supporting the role of SRSF1 in promoting LUC7L3 protein translation. We also observed a positive correlation between SRSF1 and LUC7L3 protein levels in different cell lines (Supplemental Fig. 5B). In conclusion, our findings suggest that SRSF1 depletion leads to a decrease in LUC7L3 protein levels through a mechanism involving impaired protein translation efficiency. The positive correlation between SRSF1 and LUC7L3 protein levels further supports the regulatory role of SRSF1 in LUC7L3 level.

2.5. LUC7L3 overexpression could partially rescue SRSF1 depletion-induced R-loop accumulation and abnormal spindle assembly

Given that both LUC7L3 and SRSF1 play similar roles in R-loop accumulation and spindle assembly, and that SRSF1 positively regulates LUC7L3 protein translation, we investigated whether the role of SRSF1 in LUC7L3 protein translation contributes to the regulation of genomic stability by SRSF1. We examined the intensity of R-loops in SRSF1-depleted cells and found that overexpression of LUC7L3 partially rescued the R-loop accumulation induced by SRSF1 depletion (Fig. 6A

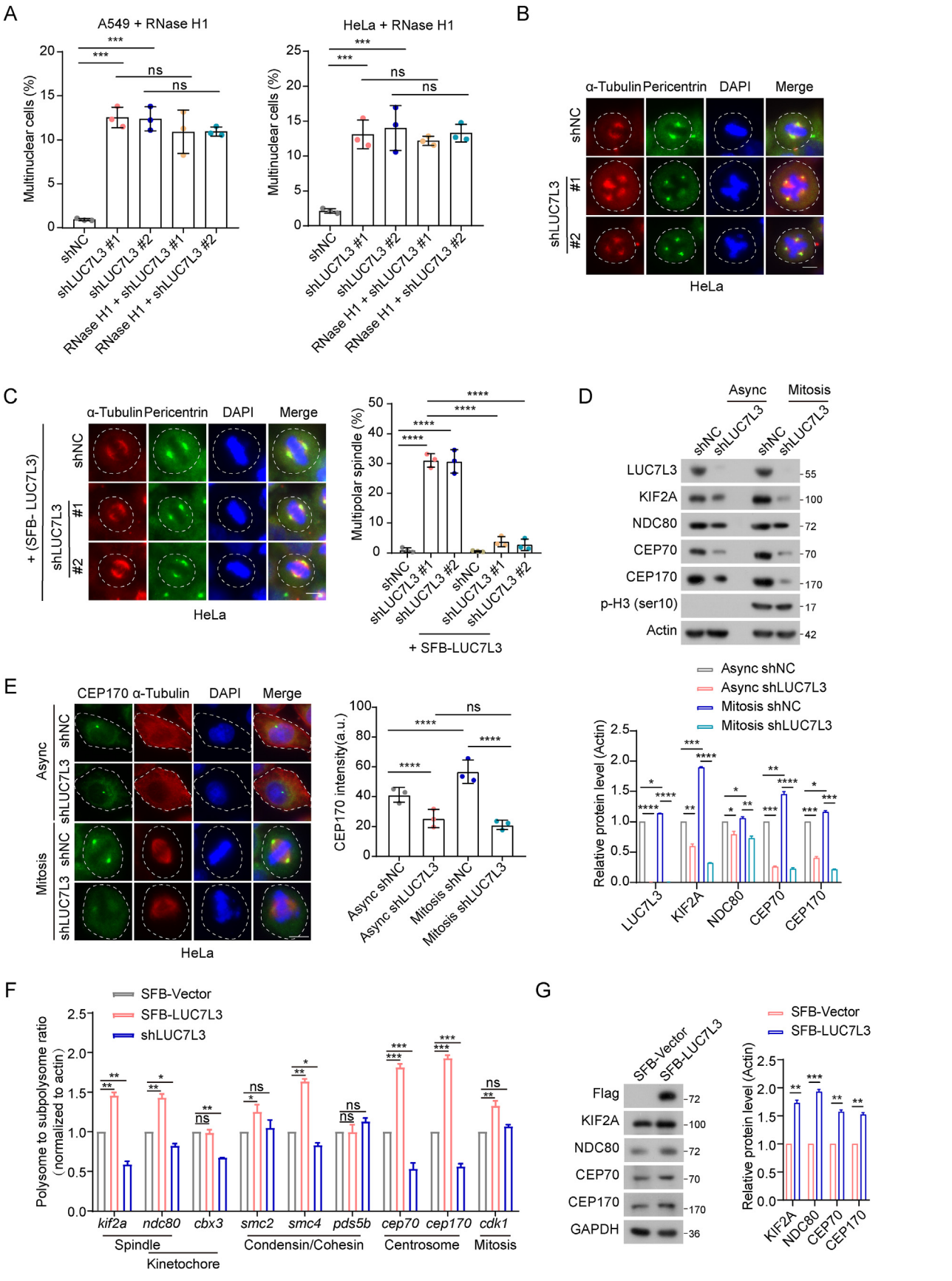

(caption on next page)

Fig. 4. Contribution of LUC7L3 to spindle assembly through promoting spindle-associated protein translation

A. Observation of cell multinucleation in LUC7L3-knockdown and GFP-RNase H1-rescued A549 and HeLa cells. Statistical analysis of the number of multinucleated cells was shown. $n > 100$.

B. Immunofluorescence analysis of mitotic spindles in LUC7L3-depleted HeLa cells. Red fluorescence indicates alpha-tubulin, green fluorescence indicates pericentrin, and blue indicates the nucleus stained with DAPI.

C. Immunofluorescence analysis of mitotic spindles in LUC7L3-depleted and SFB-LUC7L3-rescued HeLa cells. Statistical analysis of the proportion of cells with multipolar spindles was shown. $n > 100$.

D. Western blot analysis of protein levels of LUC7L3, KIF2A, NDC80, CEP70, and CEP170 in LUC7L3-depleted A549 cells. The protein level was analyzed in asynchronized cells and nocodazole-synchronized mitotic cells. Statistical quantification of each protein was shown. Asyn: Asynchronous.

E. Immunofluorescence analysis of intracellular CEP170 fluorescence in LUC7L3-depleted HeLa cells. Statistical analysis of CEP170 fluorescence signals were shown. $n > 40$. a. u. means arbitrary units.

F. Ribosomal fraction isolation assay in A549 cells overexpressing SFB-LUC7L3 or with LUC7L3 depletion. The ratio of indicated mRNA in polysome fractions to sub-polysome fractions was explored using qPCR. Statistical analysis of the ratio for each gene was shown.

G. Western blot analysis of protein levels of KIF2A, NDC80, CEP70, and CEP170 in A549 cells overexpressing SFB-SRSF1. Statistical quantification of each protein was shown. $^{*}p < 0.05$, $^{**}p < 0.01$, $^{***}p < 0.001$, $^{****}p < 0.0001$, indicating statistical significance and ns indicates non-significance. Scale bar: 10 μm. Dash lines outlined cell shape.

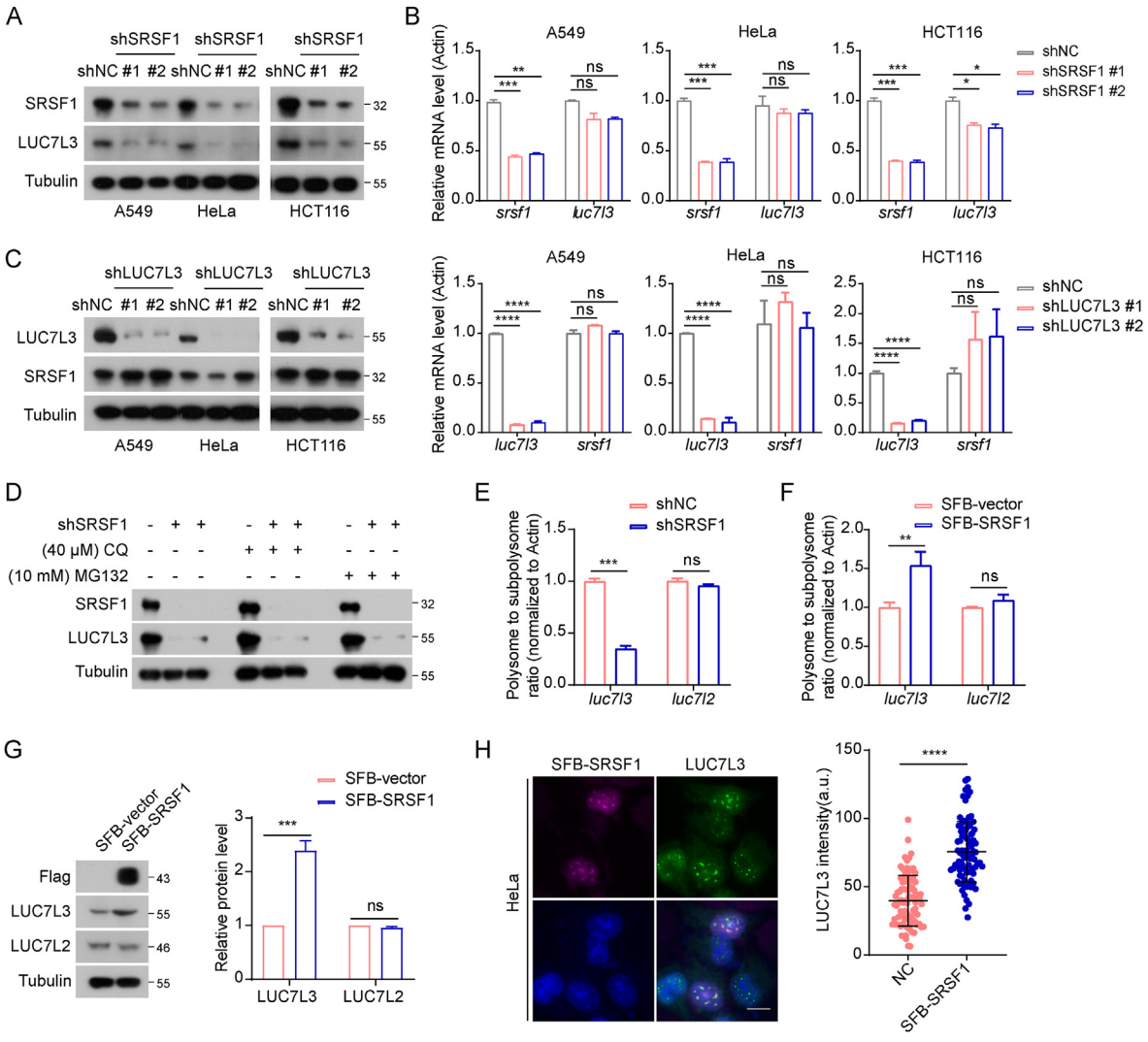

Fig. 5. SRSF1 regulates the protein translation efficiency of LUC7L3

A. Western blot analysis of LUC7L3 after SRSF1 depletion in A549, HeLa, and HCT116 cells.

B. qPCR analysis of SRSF1 and LUC7L3 mRNA levels after SRSF1 or LUC7L3 depletion in A549, HeLa, and HCT116 cells.

C. Western blot analysis of intracellular SRSF1 protein levels after LUC7L3 depletion in A549, HeLa, and HCT116 cells.

D. Western blot analysis of LUC7L3 after SRSF1 depletion in HeLa cells treated with the proteasome inhibitor MG132 or chloroquine (CQ).

E. qPCR analysis of the ratio of LUC7L3 and LUC7L2 in polysome fractions to sub-polysome fractions in LUC7L3-depleted HeLa cells.

F. qPCR analysis of the ratio of LUC7L3 and LUC7L2 in polysome fractions to sub-polysome fractions in SFB-SRSF1-overexpressing HeLa cells.

G. Western blot analysis of LUC7L3 and LUC7L2 protein levels in SFB-SRSF1-overexpressing HeLa cells.

H. Immunofluorescence analysis of endogenous LUC7L3 protein (Green) expression in HeLa cells overexpressing SFB-SRSF1 (Magenta). Blue indicates the nucleus stained with DAPI. $n > 70$. a. u. means arbitrary units. $^{*}p < 0.05$, $^{**}p < 0.01$, $^{***}p < 0.001$, $^{****}p < 0.0001$, indicating statistical significance and ns indicates non-significance. Scale bar: 10 μm.

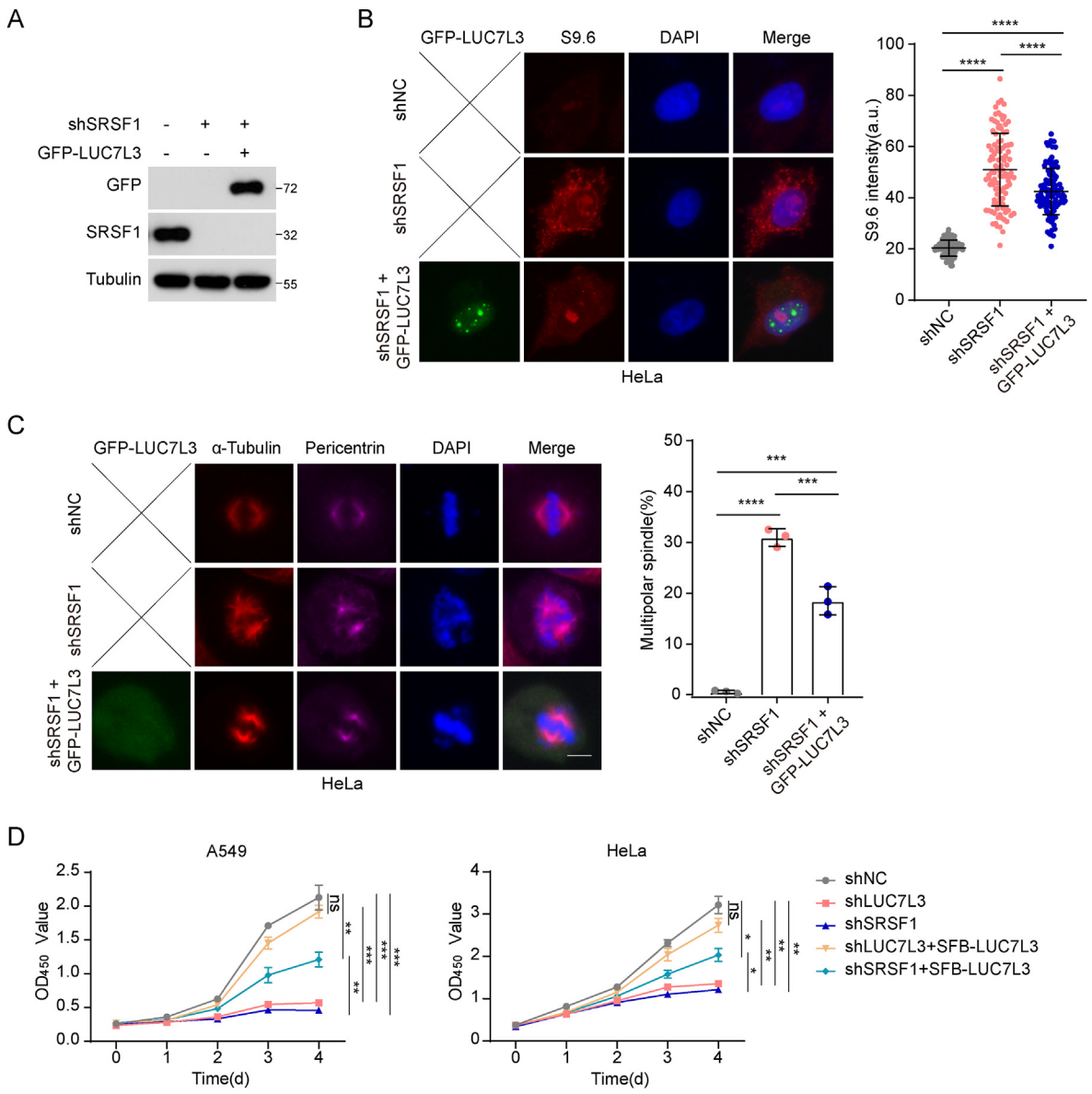

Fig. 6. Partial rescue of defects induced by SRSF1 depletion by LUC7L3 overexpression

A. Western blot analysis of SRSF1 knockdown and GFP-LUC7L3 overexpression in HeLa cells.

B. Immunofluorescence analysis of SRSF1-depleted HeLa cells with or without SFB-LUC7L3 overexpression by indicated antibodies. Red indicates S9.6 (marker for R-loops), green indicates GFP-LUC7L3, and blue indicates the nucleus stained with DAPI. Fluorescence intensity of S9.6 were analyzed using ImageJ software. $n > 100$. a. u. means arbitrary units.

C. Immunofluorescence analysis of mitotic SRSF1-depleted HeLa cells with or without SFB-LUC7L3 overexpression by indicated antibodies. Red indicates alpha-tubulin, magenta indicates pericentrin, green indicates GFP-LUC7L3, and blue indicates the nucleus stained with DAPI. Proportional analysis of cells with multipolar spindles was shown. n > 70.

D. Cell proliferation assays in A549 and HeLa cells. LUC7L3 or SRSF1-depleted cells were transfected with SFB-LUC7L3. The cell proliferation was measured using CCK-8 assay. $*p < 0.05$, $**p < 0.01$, $***p < 0.001$, $****p < 0.0001$, indicating statistical significance and ns indicates non-significance. Scale bar: 10 μm.

and B). Additionally, LUC7L3 overexpression led to a significant decrease in the formation of multipolar spindles in SRSF1-depleted cells (Fig. 6C). These findings suggest that the defects induced by SRSF1 depletion can be partially attributed to the decrease in LUC7L3 protein levels.

Furthermore, we investigated whether LUC7L3 overexpression could rescue the cell proliferation defects induced by SRSF1 depletion. Consistently, SRSF1 depletion had a similar effect on cell proliferation as LUC7L3 depletion in HeLa and A549 cells (Fig. 6D). However, LUC7L3 overexpression significantly rescued the defects induced by LUC7L3 depletion, whereas it only partially rescued the defects induced by SRSF1 depletion (Fig. 6D). This indicates that the regulation of LUC7L3 protein by SRSF1 is partially involved in the cell survival defects induced by SRSF1 depletion. Overall, our findings identify LUC7L3 as a novel downstream factor of SRSF1, contributing to the regulation of genomic stability and cell survival.

3. Discussion

Vertebrates have three Luc7p paralogs, namely LUC7L, LUC7L2, and LUC7L3, and the functions of the mammalian LUC7-like family of proteins have not been fully understood. In this study, we aimed to investigate the impact of depleting each protein on cell proliferation. Surprisingly, we found that only the depletion of LUC7L3 significantly reduced cell proliferation. Further investigations revealed that LUC7L3

depletion resulted in the accumulation of R-loops, DNA replication stress, and genomic instability. This, in turn, triggered cell apoptosis and senescence. Additionally, LUC7L3 depletion caused abnormalities in spindle assembly and the formation of multinuclear cells, likely due to dysregulated translation of proteins involved in spindle organization. Interestingly, we discovered that LUC7L3 is regulated by SRSF1, a protein known to be involved in RNA processing. SRSF1 positively regulated the translation of LUC7L3 protein, suggesting a potential interplay between these two factors.

Among the three Luc7p paralogs, only the depletion of LUC7L3 led to an accumulation of R-loops, indicating that LUC7L3 has distinct functions in R-loop formation. We also investigated the role of RBM25, a known RNA-binding protein associated with LUC7L3 (Gao et al., 2011; Zhou et al., 2008), in R-loop accumulation. Interestingly, the depletion of RBM25 did not result in significant R-loop enrichment, suggesting that the function of LUC7L3 in R-loop formation is independent of RBM25. In a recent study by Daniels et al. they analyzed the RNA binding profiles of LUC7-like proteins using seCLIP-seq (Daniels et al., 2021) and found that LUC7L2 and LUC7L3 predominantly bound to exonic sequences, which differed from the binding pattern of LUC7L. Notably, the binding pattern of LUC7L2 and LUC7L3 was similar to that of SRSF1, an RNA-binding protein containing RS domains. Given that aberrant expression of SRSF1 has been associated with R-loop-mediated genomic instability, it is possible that LUC7L3 regulates R-loop enrichment through a similar mechanism as SRSF1. Furthermore, the analysis of crosslinking site enrichment revealed that LUC7L3 had a significantly higher number of reproducible and significant crosslinking sites compared to LUC7L and LUC7L2. Specifically, LUC7L3 had 4473 crosslinking sites, while LUC7L and LUC7L2 had 385 and 260 crosslinking sites, respectively (Daniels et al., 2021) This suggests that LUC7L3 may regulate a broader range of mRNA maturation processes compared to the other two paralogs. Taken together, these findings suggest that LUC7L3 depletion induces more severe defects in mRNA maturation, potentially explaining the differences observed in R-loop accumulation compared to the other two paralogs. The distinct functions of LUC7L3 in R-loop formation and mRNA maturation highlight its unique role in cellular processes related to genome stability and RNA processing.

We also found that the depletion of LUC7L3 resulted in the formation of multipolar spindles. Specifically, we observed abnormal spindle assembly and the presence of multinucleated cells in LUC7L3-depleted cells, whereas this was not observed in LUC7L2-depleted cells. Through western blotting and IF assays, we observed a decrease in spindle-associated proteins such as CEP170, CEP70, and KIF2A in LUC7L3-depleted cells. This suggests that LUC7L3 may regulate the translation of various spindle-associated proteins. LUC7L3 depletion induced a more severe decrease of these proteins in nocodazole-synchronized mitotic cells, indicating the function of LUC7L3 on protein translation tended to occur in G2 or mitotic cells. Further experiments are required to elucidate the underlying mechanism behind the effect of LUC7L3 on protein translation, which will help to precisely define the role of LUC7L3 in protein translation in interphase cells and mitotic cells. Interestingly, the function of LUC7L3 in spindle assembly was similar to that of SRSF1, indicating that LUC7L3 and SRSF1 may regulate protein translation through the same mechanism. Considering the interaction between SRSF1 and LUC7L3 (Umehara et al., 2003), as well as the role of SRSF1 in enhancing the translation efficiency of LUC7L3, it is reasonable to propose that LUC7L3 collaborates with SRSF1 to facilitate its own translation efficiency. Hence, it is crucial to unravel the underlying mechanism governing LUC7L3's impact on protein translation. Previous studies have demonstrated the role of SRSF1 in protein translation processes. For instance, SRSF1 has been shown to associate with translating ribosomes and stimulate translation in Xenopus oocytes. It also enhances the translation of reporter mRNAs in HeLa cells (Sanford et al., 2004). Additionally, SRSF1 regulates translation initiation by enhancing the phosphorylation of 4E-BP1 (Michlewski et al., 2008). It binds to LIG1 mRNA and regulates its expression in an mTOR-dependent manner by increasing its mRNA stability and enhancing its translation (Martinez-Terroba et al., 2018). Further experiments are needed to determine if LUC7L3 also functions in these processes.

Given the shared functions of LUC7L3 and SRSF1 in R-loop formation and spindle assembly, we investigated the relationship between these two proteins. Surprisingly, we found that SRSF1 positively regulates the protein level of LUC7L3, but not LUC7L2, by promoting its translation. This suggests that LUC7L3 is a downstream factor of SRSF1. We also explored whether the decrease in LUC7L3 in SRSF1-depleted cells contributes to the defects in R-loop accumulation and spindle assembly. Overexpressing LUC7L3 in SRSF1-depleted cells partially rescued the defects in R-loop and spindle assembly, indicating that LUC7L3 plays a role in these processes. Since SRSF1 has been reported to interact with LUC7L3, it is possible that SRSF1 and LUC7L3 form a complex to regulate alternative splicing and protein translation.

In summary, our study highlights the distinct functions of LUC7L3 in cell proliferation, R-loop formation, spindle assembly, and genome stability. Depletion of LUC7L3 may lead to severe defects in mRNA maturation, resulting in the accumulation of R-loops. This accumulation of R-loops caused by LUC7L3 depletion collides with DNA replication machinery, leading to replication stress and genomic instability (Fig. 7). Moreover, we also provide insights into the interplay between LUC7L3 and SRSF1. We found that SRSF1 positively regulates the protein levels of LUC7L3 by enhancing its translation. Interestingly, LUC7L3 is also involved in regulating the mRNA translation of genes related to mitotic spindle assembly, similar to the role of SRSF1 in protein translation (Fig. 7). These findings contribute to our understanding of the complex regulatory networks involved in genome stability, mRNA processing, and cellular proliferation.

4. Material and methods

4.1. Cell culture and cell cycle synchronization

A549, HeLa, HCT116, RPE (hTERT RPE-1), and HEK293T cells were obtained from the American Type Culture Collection (ATCC, http://www.atcc.org) and cultured in Dulbecco's modified Eagle's medium (DMEM) with high glucose. The medium was supplemented with 10% fetal bovine serum and 100 U/mL penicillin and 0.1 mg/mL streptomycin.

Cells were synchronized into the S phase using a double thymidine block. Briefly, the cells were initially blocked with 2 mM thymidine for 18 h. They were then released into fresh media for 9 h before being treated with thymidine again for 15 h. After this, the cells were released for an additional 5 h. To synchronize cells at the M phase, HeLa cells were treated with 2 mM thymidine for 24 h. Subsequently, they were treated with 200 nM nocodazole for 11 h.

4.2. Plasmid transfection

Plasmids expressing SFB-LUC7L3, SFB-SRSF1, and GFP-RNase H1 were prepared for transfection experiments. A 3:1 ratio of polyethyleneimine (PEI) transfection reagent (Sigma) to plasmid DNA was used for transfection in subsequent experiments.

shRNA targeting LUC7L3, SRSF1, LUC7L, LUC7L2, RBM25, and a negative control shRNA (shNC) were inserted into the pLKO.1 lentiviral vector. The shRNA-pLKO.1 constructs were co-transfected with pSPAX2 and pMD2. G into HEK293T cells for lentivirus production. HeLa, A549, and HCT116 cells were selected in the presence of 2 μg/mL puromycin, while RPE cells were selected in the presence of 5 μg/mL puromycin. The target sequences for LUC7L3 knockdown were as follows 5′-CCGGGATCGAAAGTCATATAA-3′ for shLUC7L3 #1, and 5′-GCGATACTTACAGAGCTTACT-3′ for shLUC7L3 #2. Target sequences for SRSF1 knockdown were as follows 5′-GAAGCAGGTGATGTATGTTAT-3′ for shSRSF1 #1, and 5′-ACTTACCTCCAGACATCCGAA-3′ for shSRSF1 #2. Target sequences for RBM25 knockdown were as follows 5′-GCGCCTTAAGAATTGGGAAAT-3′ for shRBM25 #1, and 5′-

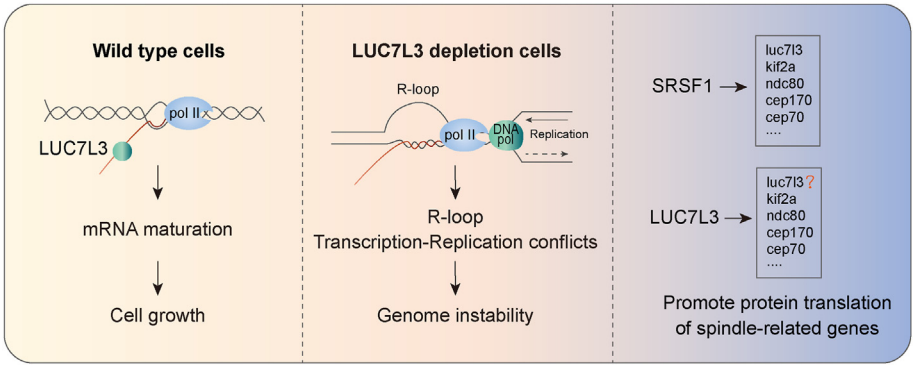

Fig. 7. Model for the function of LUC7L3
Depletion of LUC7L3 may lead to severe defects in mRNA maturation, resulting in the accumulation of R-loops. This accumulation of R-loops caused by LUC7L3 depletion may collide with DNA replication machinery, leading to replication stress and genomic instability. Moreover, SRSF1 positively regulates the protein levels of LUC7L3 by enhancing its translation. LUC7L3 is also involved in regulating the mRNA translation of genes related to mitotic spindle assembly, similar to the role of SRSF1 in protein translation.

GGAAAGCATTTGGGCGCAAGA -3′ for shRBM25. Target sequences for LUC7L knockdown were as follows 5′-CCAGACAGAGGGTCAAGTTTA-3′ for shLUC7L #1, and 5′-GGAGTCCTTTATTGCTGAATG-3′ for shLUC7L #2. Target sequences for LUC7L2 knockdown were as follows 5′-GCAGAGGAAGTTATCGGAAT-3′ for shLUC7L2 #1, and 5′-GTAATGGATGAAGTAGAGAAA-3′ for shLUC7L2 #2.

4.3. Immunoprecipitation and western blot

Protein from each cell line was extracted by using NETN420 lysis buffer (420 mM NaCl, 20 mM Tris-HCl, pH 8.0, 1 mM EDTA, 0.5% NP-40 and 1 × protease inhibitor cocktail). Cell lysates were centrifuged at 15,000 rpm for 15 min at 4 °C and the supernatants were collected. Proteins were denatured by boiling in SDS loading buffer for 10 min. For immunoprecipitation, the antibody-conjugated Protein G beads (MCE) were mixed with cell extracts for 2 h at 4 °C.The beads were washed five times with NETN100 buffer (100 mM NaCl, 20 mM Tris-HCl, pH 8.0, 1 mM EDTA, 0.5% NP-40), and then resuspended in SDS loading buffer, followed by denaturation and elution in 95 °C for 10 min.

Protein samples were separated by SDS-PAGE and transferred onto PVDF membrane. The following primary antibodies were used LUC7L3 (Proteintech, 14504-1-AP), SRSF1 (Abcam, ab38017), Flag (Sigma, F9291), GFP (Proteintech, 50430-2-AP), KAP1 (Cell Signaling Technology, #4123), p-KAP1(S824) (Abcam, ab133440), CHK1 (Cell Signaling Technology, #37010), p-CHK1(S345) (Cell Signaling Technology, #2348S), γH2AX (Abcam, ab81299), NDC80 (Proteintech, 25297-1-AP), CEP170 (Proteintech, 18899-1-AP), CEP70 (Proteintech, 16280-1-AP), KIF2A (Proteintech, 13105-1-AP), LUC7L (Abcam, ab91294), LUC7L2 (Proteintech, 25297-1-AP), RBM25 (Proteintech, 25297-1-AP), Tubulin (Proteintech, 10094-1-AP), GAPDH (Proteintech, 60004-1-Ig), Actin (Proteintech, 60009-1-Ig).

4.4. Immunofluorescence analysis

Adherent cells were grown on sterile glass coverslips in a 24-well cell culture plate. Cells were fixed with pre-cooled 4% paraformaldehyde for 15 min, permeabilized in 0.5% Triton X-100 for 5 min, blocked with 5% BSA for 30 min, incubated with primary antibody diluted with 5% BSA for 2 h. After washing 3 times with PBS, the coverslips were incubated with secondary antibody diluted with 5% BSA for 1 h in the dark. Subsequently, the coverslips were washed three times with PBS, followed by incubation with DAPI for 5 min in the dark and washed three times with PBS.

For S9.6 (R-loop) detection, cells were fixed with ice-cold methanol for 10 min followed by acetone exposure for 1 min on ice, blocked with 3% BSA, and incubated with S9.6 primary and secondary antibodies in 4 × SCC buffer (NaCl, sodium citrate 0.1% Tween, pH 7.0). The slides were then incubated with DAPI for 5 min in the dark. Slides were washed three times with PBS, mounted with Fluoromount-G (Southern Biotech), dried, imaged under an Olympus microscope and images were analyzed using Image J software.

4.5. DNA fiber assay

Cells were synchronized to the S phase by double thymidine block. Subsequently, CIdU (25 μM) was added for 20 min, followed by IdU (250 μM) for a further 40 min. Cells were harvested and washed twice with PBS. Cell samples of 2 μL (1,000 cells) were spotted onto the glass slide, air-dried for 5 min, and lysed in 7 μL lysis buffer (200 mM Tris-HCl, pH 7.5, 50 mM EDTA, 5% SDS) for 2 min. The slide was placed at an angle of 30 °C to allow the DNA to flow out slowly. Slides were air dried before fixation in methanol: acetic acid (3:1). Fixed fibers were denatured in 2.5 M HCl for 1 h before blocking in 5% BSA for 1 h and then incubated with anti-mouse BrdU antibody (BD Biosciences, 1:60), and anti-rabbit BrdU antibody (Sigma, 1:500) for 2 h, respectively. Slides were washed three times with 0.05% Tween-20 and PBS, followed by incubation with Alexa Fluor 488-conjugated goat anti-rat antibody (Thermo Fisher Scientific, 1:400) and Alexa Fluor 647-conjugated goat anti-mouse secondary antibody (Thermo Fisher Scientific, 1:400) for 1 h in the dark. Slides were washed three times with 0.05% Tween-20 and PBS. Slides were imaged using an Olympus microscope and the track lengths of the labeled replication forks were analyzed manually using Image J software.

4.6. Chromosome spreading

Cells were treated with 200 nM nocodazole to block in mitosis. The rounded cells were vortexed and collected. 75 mM KCl hypotonic solution was added for 30 min at 37 °C before centrifugation at 300*g* for 4 min at 4 °C. The pellets were then resuspended in ice-cold methanol: glacial acetic acid (3:1) for fixation for 5 min. After removal of the fixation reagents, the cell suspension was dropped onto a slide moistened with acetic acid to spread the metaphase chromosomes. The spreads were air-dried and stained with Giemsa solution (Solarbio) for 15 min. Images were captured using an Olympus microscope.

4.7. Fluorescence quantitative PCR

2 × Chamq SYBR colour qPCR Master Mix (Vazyme) was used for the fluorescence quantitative PCR reaction. Each group of experimental data was repeated three times, and the data were stored. $2^{-\triangle\triangle ct}$ was used for calculation and GraphPad Prism 8.0.1 was used for data analysis. qPCR primers are listed in Table S1.

4.8. Cell growth assay

To measure cell growth of LUC7L3 knockdown cells, cells were infected with lentivirus expressing shRNA for 48 h, seeded in a 96-well

plate at 2,000 cells/well and adherently cultured for 24, 48, 72 and 96 h. Each well was incubated with Cell Counting Kit-8 reagent solution (Zoman Biotechnology) for 2 h in the dark. Absorbance at 450 nm was measured using a microplate reader (Spectramax i3x). The cell viability rate was calculated, and the cell viability curve was plotted using GraphPad Prism 8.0.1 software.

4.9. Colony formation assays

Cells were infected with lentivirus expressing shLUC7L3 for 48 h, seeded in a 6-well plate at 300 cells/well, with 3 replicate wells each, and maintained in the cell culture incubator for 10 days of adherent culture, with fresh medium added every 3 days. When the cells had grown to visible cell clones, the old culture medium was discarded, and the cells were washed twice with PBS. Cells were fixed with pre-cooled anhydrous methanol for 20 min, and 0.5% crystal violet was prepared in anhydrous methanol and stained for 30 min. The staining solution was discarded, rinsed with water and the images were saved. Colonies were calculated using GraphPad Prism 8.0.1 software.

4.10. Cell apoptosis

For apoptosis analysis, 72 h after infection with lentivirus expressing shLUC7L3 #1, shLUC7L3 #2, or shNC, A549 and HeLa cells were harvested and washed twice with PBS. Cells were stained with Annexin-V FITC and PI (Zoman Biotechnology). The cell samples were analyzed by flow cytometry (BD) and FlowJo software.

4.11. Cell senescence

Cell senescence was detected using the Cell Senescence β-Galactosidase Staining Kit (Beyotime Biotechnology). Cells were infected with lentivirus expressing shLUC7L3 for 72 h. The old cell culture medium was discarded, 1 mL of β-galactosidase staining fixative was added and the cells were fixed for 15 min. The cell fixative was discarded and added staining solution. The cells were incubated overnight at 37 °C in a thermostat. The image was captured under a light microscope. The cell senescence rate was calculated using GraphPad Prism 8.0.1 software.

4.12. Polysome profiling assay

Prior to harvest, cells were treated with 100 μg/mL CHX at 37 °C for 15 min to block translation, and cells were washed twice with PBS containing CHX. Cells were then collected by digestion and transferred to new EP tubes. Each sample was lysed with 800 μL cell lysis buffer (sucrose gradient solution containing 0.5% NP-40, 0.1% CHX, 1% protease inhibitor cocktail, 0.125% RNase inhibitor) for 20 min on ice, and the extracts were inverted and mixed every 5 min until complete lysis. After centrifugation at 12,000*g* at 4 °C for 15 min, the supernatant was transferred to a fresh centrifuge tube. Lysates were layered onto 10–60% sucrose gradient buffer containing 2.2 M sucrose, 1 M Tris-HCl, pH 7.5, 5 M NaCl and 1 M $MgCl_2$, which were prepared using a density gradiometer. The gradients were centrifuged at 4 °C, 39,000 rpm for 90 min, the fractionation apparatus was set up and 1 mL of each sample was collected every 1 min, the gradient curve of the RNA was collected by continuously monitoring the absorbance at 260 nm. 12 tubes were collected and marked for subsequent experiments or frozen at −80 °C. Phenol-chloroform extraction of RNA was followed by qPCR detection. The ratio of indicated mRNA in polysome fractions and sub-polysome fractions was used to indicate the protein translation efficiency.

4.13. Statistical analysis

For grayscale analysis in Fig. 4D and G, protein level of each spindle-related gene was quantified to the level of indicated loading control. The relative mean gray value of each spindle-related protein in wild-type asynchronized cells was set as 1. Statistical analysis was performed using GraphPad Prism 8.0.1 software. A Student's t-test was performed for unpaired samples. Results are displayed as mean ± SD in graphs. Significance is represented as * $p < 0.05$, *** $p < 0.01$, *** $p < 0.001$, **** $p < 0.0001$, ns indicates non-significance. ($p > 0.05$). All data were replicated three times in the study.

Author contributions

QC designed and supervised the study. X-QZ performed all the experiments and analyzed the data. XZ and XS performed polysome profiling assay. QC, X-QZ and JG wrote the manuscript.

Declaration of competing interest

The authors declare no competing financial interests.

Acknowledgements

Q. Chen is supported by grants from the National Natural Science Foundation of China (32170698) and the Fundamental Research Funds for the Central Universities (2042022dx0003).

Appendix A. Supplementary data

Supplementary data to this article can be found online at https://doi.org/10.1016/j.cellin.2024.100170.

References

Agarwal, R., Schwer, B., & Shuman, S. (2016). Structure-function analysis and genetic interactions of the Luc7 subunit of the Saccharomyces cerevisiae U1 snRNP. *Rna, 22*(9), 1302–1310.
Aguilera, A., Garcia-Muse, T., & Loops, R. (2012). From transcription byproducts to threats to genome stability. *Molecular Cell, 46*(2), 115–124.
Bayona-Feliu, A., et al. (2021). The SWI/SNF chromatin remodeling complex helps resolve R-loop-mediated transcription-replication conflicts. *Nature Genetics, 53*(7), 1050–+.
Bhatia, V., et al. (2014). BRCA2 prevents R-loop accumulation and associates with TREX-2 mRNA export factor PCID2. *Nature, 511*(7509), 362-+.
Boguslawski, S. J., et al. (1986). Characterization of monoclonal-antibody to DNA.rna and its application to immunodetection of hybrids. *Journal of Immunological Methods, 89*(1), 123–130.
Bou-Nader, C., et al. (2022). Structural basis of R-loop recognition by the S9.6 monoclonal antibody. *Nature Communications, 13*(1).
Cerritelli, S. M., & Crouch, R. J. (2009). Ribonuclease H: The enzymes in eukaryotes. *FEBS Journal, 276*(6), 1494–1505.
Cerritelli, S. M., Sakhuja, K., & Crouch, R. J. (2022). RNase H1, the gold standard for R-loop detection. *Methods in Molecular Biology, 2528*, 91–114.
Chakraborty, A., et al. (2020). Replication stress induces global chromosome breakage in the fragile X genome. *Cell Reports, 32*(12).
Chakraborty, P., Huang, J. T. J., & Hiom, K. (2018). DHX9 helicase promotes R-loop formation in cells with impaired RNA splicing. *Nature Communications, 9*.
Chen, L., et al. (2018). The augmented R-loop is a unifying mechanism for myelodysplastic syndromes induced by high-risk splicing factor mutations. *Molecular Cell, 69*(3), 412-+.
Chodosh, L. A., et al. (1989). 5,6-Dichloro-1-beta-D-ribofuranosylbenzimidazole inhibits transcription elongation by RNA polymerase II in vitro. *Journal of Biological Chemistry, 264*(4), 2250–2257.
Daniels, N. J., et al. (2021). Functional analyses of human LUC7-like proteins involved in splicing regulation and myeloid neoplasms. *Cell Reports, 35*(2), Article 108989.
Gan, W. J., et al. (2011). R-loop-mediated genomic instability is caused by impairment of replication fork progression. *Genes & Development, 25*(19), 2041–2056.
Gao, G., & Dudley, S. C. (2013). RBM25/LUC7L3 function in cardiac sodium channel splicing regulation of human heart failure. *Trends in Cardiovascular Medicine, 23*(1), 5–8.
Gao, G., et al. (2011). Role of RBM25/LUC7L3 in abnormal cardiac sodium channel splicing regulation in human heart failure. *Circulation, 124*(10), 1124-U112.
Goulielmaki, E., et al. (2021). The splicing factor XAB2 interacts with ERCC1-XPF and XPG for R-loop processing. *Nature Communications, 12*(1).
Halliwell, J. A., Gravells, P., & Bryant, H. E. (2020). DNA fiber assay for the analysis of DNA replication progression in human pluripotent stem cells. *Curr Protoc Stem Cell Biol, 54*(1), e115.
Hamperl, S., & Cimprich, K. A. (2014). The contribution of co-transcriptional RNA:DNA hybrid structures to DNA damage and genome instability. *DNA Repair, 19*, 84–94.
Hamperl, S., et al. (2017). Transcription-replication conflict orientation modulates R-loop levels and activates distinct DNA damage responses. *Cell, 170*(4), 774-+.

Hodroj, D., et al. (2017). An ATR-dependent function for the Ddx19 RNA helicase in nuclear R-loop metabolism. *Embo Journal, 36*(9), 1182–1198.
Howell, V. M., et al. (2007). Evidence for a direct role of the disease modifier SCNM1 in splicing. *Human Molecular Genetics, 16*(20), 2506–2516.
Jimenez, M., et al. (2019). Splicing events in the control of genome integrity: Role of SLU7 and truncated SRSF3 proteins. *Nucleic Acids Research, 47*(7), 3450–3466.
Jin, B., et al. (2023). MEN1 is a regulator of alternative splicing and prevents R-loop-induced genome instability through suppression of RNA polymerase II elongation. *Nucleic Acids Research*.
Jourdain, A. A., et al. (2021). Loss of LUC7L2 and U1 snRNP subunits shifts energy metabolism from glycolysis to OXPHOS. *Mol Cell, 81*(9), 1905–1919 e12.
Khanna, K. K., & Jackson, S. P. (2001). DNA double-strand breaks: Signaling, repair and the cancer connection. *Nature Genetics, 27*(3), 247–254.
Le Sénéchal, R., et al. (2023). Alternative splicing of BCL-x is controlled by RBM25 binding to a G-quadruplex in BCL-x pre-mRNA. *Nucleic Acids Research*.
Li, C., et al. (2021). The RNA-binding protein LUC7L2 mediates MITA/STING intron retention to negatively regulate innate antiviral response. *Cell Discov, 7*(1), 46.
Li, X. L., & Manley, J. L. (2005). Inactivation of the SR protein splicing factor ASF/SF2 results in genomic instability. *Cell, 122*(3), 365–378.
Li, X. L., Niu, T. H., & Manley, J. L. (2007). The RNA binding protein RNPS1 alleviates ASF/SF2 depletion-induced genomic instability. *Rna, 13*(12), 2108–2115.
Lin, W. L., et al. (2022). DDX18 prevents R-loop-induced DNA damage and genome instability via PARP-1. *Cell Reports, 40*(3).
Mah, L. J., El-Osta, A., & Karagiannis, T. C. (2010). γH2AX: A sensitive molecular marker of DNA damage and repair. *Leukemia, 24*(4), 679–686.
Martinez-Terroba, E., et al. (2018). The oncogenic RNA-binding protein SRSF1 regulates LIG1 in non-small cell lung cancer. *Laboratory Investigation, 98*(12), 1562–1574.
Maslon, M. M., et al. (2014). The translational landscape of the splicing factor SRSF1 and its role in mitosis. *Elife, 3*, Article e02028.
Matos, D. A., et al. (2020). ATR protects the genome against R loops through a MUS81-triggered feedback loop. *Molecular Cell, 77*(3), 514-+.
Michalet, X., et al. (1997). Dynamic molecular combing: Stretching the whole human genome for high-resolution studies. *Science, 277*(5331), 1518–1523.
Michlewski, G., Sanford, J. R., & Cáceres, J. F. (2008). The splicing factor SF2/ASF regulates translation initiation by enhancing phosphorylation of 4E-BP1. *Mol Cell, 30*(2), 179–189.
Minocherhomji, S., et al. (2015). Replication stress activates DNA repair synthesis in mitosis. *Nature, 528*(7581), 286-+.
Niehrs, C., & Luke, B. (2020). Regulatory R-loops as facilitators of gene expression and genome stability. *Nature Reviews Molecular Cell Biology, 21*(3), 167–178.
Nishii, Y., et al. (2000). CROP/Luc7A, a novel serine/arginine-rich nuclear protein, isolated from cisplatin-resistant cell line. *FEBS Letters, 465*(2–3), 153–156.
Prasad, J., et al. (1999). The protein kinase Clk/Sty directly modulates SR protein activity: Both hyper- and hypophosphorylation inhibit splicing. *Molecular and Cellular Biology, 19*(10), 6991–7000.
Prendergast, L., et al. (2020). Resolution of R-loops by INO80 promotes DNA replication and maintains cancer cell proliferation and viability. *Nature Communications, 11*(1).
Redon, C., et al. (1999). Megabase chromatin domains involved in DNA double-strand breaks. *Molecular Biology of the Cell, 10*, 282a-282a.
Roberts, R. W., & Crothers, D. M. (1992). Stability and properties of double and triple helices - dramatic effects of rna or DNA backbone composition. *Science, 258*(5087), 1463–1466.
Rogakou, E. P., et al. (1998). DNA double-stranded breaks induce histone H2AX phosphorylation on serine 139. *Journal of Biological Chemistry, 273*(10), 5858–5868.
Sanford, J. R., et al. (2004). A novel role for shuttling SR proteins in mRNA translation. *Genes Dev, 18*(7), 755–768.
Stein, H., & Hausen, P. (1969). Enzyme from calf thymus degrading the RNA moiety of DNA-RNA hybrids: Effect on DNA-dependent RNA polymerase. *Science, 166*(3903), 393–395.
Técher, H., et al. (2013). Replication dynamics: Biases and robustness of DNA fiber analysis. *Journal of Molecular Biology, 425*(23), 4845–4855.
Thomas, M., White, R. L., & Davis, R. W. (1976). Hybridization of RNA to double-stranded DNA: Formation of R-loops. *Proc Natl Acad Sci U S A, 73*(7), 2294–2298.
Tuduri, S., et al. (2010). Topoisomerase I suppresses genomic instability by preventing interference between replication and transcription (vol 51, pg 295, 1984). *Nature Cell Biology, 12*(11), 1122-1122.
Umehara, H., et al. (2003). Effect of cisplatin treatment on speckled distribution of a serine/arginine-rich nuclear protein CROP/]Luc7A. *Biochemical and Biophysical Research Communications, 301*(2), 324–329.
Wahba, L., et al. (2011). RNase H and multiple RNA biogenesis factors cooperate to prevent RNA:DNA hybrids from generating genome instability. *Molecular Cell, 44*(6), 978–988.
White, D. E., et al. (2006). KAP1, a novel substrate for PIKK family members, colocalizes with numerous damage response factors at DNA lesions. *Cancer Research, 66*(24), 11594–11599.
Yang, Y. Z., et al. (2014). Arginine methylation facilitates the recruitment of TOP3B to chromatin to prevent R loop accumulation. *Molecular Cell, 53*(3), 484–497.
Yang, Y., et al. (2022). Transcription-replication conflicts in primordial germ cells necessitate the Fanconi anemia pathway to safeguard genome stability. *Proc Natl Acad Sci U S A, 119*(34), Article e2203208119.
Yankulov, K., et al. (1995). The transcriptional elongation inhibitor 5,6-dichloro-1-beta-D-ribofuranosylbenzimidazole inhibits transcription factor IIH-associated protein kinase. *Journal of Biological Chemistry, 270*(41), 23922–23925.
Yu, Z. B., et al. (2020). DDX5 resolves R-loops at DNA double-strand breaks to promote DNA repair and avoid chromosomal deletions. *Nar Cancer, 2*(3).
Zhou, A., et al. (2008). Novel splicing factor RBM25 modulates Bcl-x pre-mRNA 5 ' splice site selection. *Molecular and Cellular Biology, 28*(19), 5924–5936.
Ziv, Y., et al. (2006). Chromatin relaxation in response to DNA double-strand breaks is modulated by a novel ATM and KAP-1 dependent pathway. *Nature Cell Biology, 8*(8), 870-U142.